Capability of LEP-Type Surfaces To Describe Noncollinear Reactions. 2. Polyatomic Systems

J. Espinosa-García[†]

Departamento de Química Física, Universidad de Extremadura, 06071 Badajoz, Spain

Received: April 26, 2001; In Final Form: July 10, 2001

In this second article of the series, the popular LEP-type surface for collinear reaction paths and a "bent" surface, which involves a saddle point geometry with a nonlinear central angle, were used to examine the capacity of LEP-type surfaces to describe the kinetics and dynamics of noncollinear reaction paths in polyatomic systems. Analyzing the geometries, vibrational frequencies, curvature along the reaction path (to estimate the tunneling effect and the reaction coordinate-bound modes coupling), and the variational transition-state theory thermal rate constants for the $NH_3 + O(^3P)$ reaction, we found that the "collinear" LEP-type and the "bent" surfaces for this polyatomic system show similar behavior, thus allowing a considerable saving in time and computational effort. This agreement is especially encouraging for this polyatomic system because in the Cs symmetry the reaction proceeds via two electronic states of symmetries $^3A'$ and $^3A''$, which had to be independently calibrated. Finally, this work on polyatomic systems generalizes the conclusions reached in our previous article on triatomic systems, so that it therefore appears to be a general behavior for any reactive system.

1. Introduction

In a previous paper[1] using the nonlinear atom−diatom Cl + HCl system as test (Cl−H−Cl angle ≠ 180°) we showed that a typical collinear LEPS surface and a simple "bent" surface that we had constructed and calibrated present similar kinetic and dynamic behavior. This capacity of typical LEPS surfaces to reproduce the kinetics and dynamics of triatomic systems with noncollinear reaction paths is encouraging and opens up the possibility of using this simple functional form with suitable modifications as a starting point in constructing analytical potential energy surfaces (PES) for noncollinear polyatomic systems, with the consequent saving in computation time. In this latter case, we can speak of a LEP-type surface to distinguish it from the "pure" LEPS surface used for triatomic systems.

Recently, our group[2] has exhaustively studied the $NH_3 + O(^3P)$ reaction using a "direct dynamics" method,[3] which describes a chemical reaction by using ab initio electronic structure information (energies, gradients and Hessians) only in the region of configuration space along the reaction path, without the intermediary of an analytical potential energy surface fit. This reaction is particularly challenging because for the H atom abstraction reaction, the approach of the $O(^3P)$ atom to ammonia with Cs symmetry proceeds via two electronic states of symmetries $^3A'$ and $^3A''$, with a hydrogen-bonded complex in the exit channel (HBP). Indeed, for C_s symmetry the irreducible representation is $^3A' + {}^3A''$ for reactants, and $^3A' + {}^3A'' + {}^1A' + {}^1A''$ for products, and the two asymptotes therefore adiabatically correlate through the potential energy surfaces $^3A'$ and $^3A''$ in Cs. We found that both the $^3A'$ and $^3A''$ saddle points are "bent", with N−H_1−O angles of 159.5° and 144.4°, respectively, with the $^3A''$ saddle point 1.2 kcal mol^{-1} more stable than the $^3A'$ one. We also found a strong coupling of the reaction path to the NH_3 reactive stretch and umbrella modes, and, therefore, excitation of these modes might be expected to enhance the forward reaction rates. This reaction-path curvature analysis also showed that tunneling plays an important role in this reaction. In the present paper, these will be denoted as "bent" ab initio surfaces.

However, despite the enormeous computational effort, increased in this case because there are two surfaces, this method still presents limitations. For instance, it only describes the zero-point vibrational valley around the minimum energy path (MEP), but when the heavy−light−heavy (HLH) mass combination is present, as in this case, large "corner cutting" tunneling effects are possible, in which reaction-path curvature leads to internal centrifugal forces that tend to make the system leave the MEP, and tunneling paths on the concave side of the MEP are favored. To the best of our knowledge, this was the first ab initio study of this reaction, because the transition-state theory calculations of Salimian et al.[4] and Cohen[5] are really empirical approximations.

There has been a large amount of experimental work on this reaction,[4,6−18] which has been comprehensively reviewed by Cohen,[5] Baulch et al.,[19] and more recently, by Dean and Bozzelli.[20] Cohen finds that the available data are not sufficient to determine whether the initial step is H atom abstraction or O atom addition, and that the low-temperature values of the rate constant ($T \leq 400$ K) are not consistent with values deduced at higher temperatures if the reaction proceeds by H-abstraction. He recommends the expression $k(T) = 1.8 \times 10^{-18}\ T^{2.1} \exp(-2620/T)$ cm^3 molecule^{-1} s^{-1}, with a high degree of curvature ($T^{2.1}$) in the Arrhenius plot which is not evident from the experimental data. Baulch et al. recommend the Arrhenius expression $k(T) = 1.6 \times 10^{-11} \exp(-3670/T)$ over the range 500−2500 K, with an error limit of $\Delta \log K = \pm 0.5$, and Dean and Bozzelli suggest the non-Arrhenius expression $k(T) = 1.6 \times 10^{-17} T^{1.94} \exp(-3250/T)$ over the range 450−1800 K. From these surveys[5,19,20] it appears that the best values are those of Perry[14] at low temperatures [$k(T) = 3.42 \times 10^{-11} \exp(-4530/T)$ over the range 448−841 K], of Sutherland et al.[18] at intermediate temperatures [$k(T) = 1.07 \times 10^{-10} \exp(-5613/T)$

[†] E-mail: joaquin@unex.es.

10.1021/jp011594a CCC: $20.00
Published on Web 08/21/2001

over the range 765−1790 K], and of Salimian et al.[4] at high temperatures [$k(T) = 3.63 \times 10^{-11} \exp(-4470/T)$ over range 1750−2060 K], although this last presents uncertainties of 0.5k and 2.0k, i.e., a factor of 4, and, therefore it has to be taken with caution.

The disagreement concerning the curvature in the Arrhenius plot is probably simply because the experimental measurements were performed independently over different temperature ranges. However, this reaction presents a heavy−light−heavy (HLH) mass combination, which is a good candidate to present a large tunneling effect at low temperatures, and, therefore, curvature in the Arrhenius plot. Obviously, this effect will become more patent when a larger range of temperatures is analyzed simultaneously.

The previous ab initio results from our group,[2] (geometry, frequency, reaction-path analysis, and tunneling) will be used together with these experimental kinetic studies in this work for calibration purposes.

In the present work, using the noncollinear polyatomic $NH_3 + O(^3P)$ reaction as test, we report the construction of two LEP-type analytical PESs, with $^3A'$ and $^3A''$ symmetries. The comparison of the results for the kinetics and dynamics with those for the "bent" ab initio surfaces ($^3A'$ and $^3A''$) will permit us to answer to the question of whether the popular and simple LEP-type function can describe the kinetics and dynamics of polyatomic systems with "bent" saddle point geometries.

2. LEP-Type Potential Energy Surface

The first step in the PES construction is the choice of the functional forms to represent the stretching and bending modes. The construction of the $NH_3 + O(^3P)$ PES was based on the PES for the similar $NH_3 + H$ reaction from our group,[21] taking into account that both are hydrogen abstraction reactions from ammonia. This potential was formulated in terms of stretching (str), harmonic bending (harm) and umbrella bending (umb) terms, and has the form

$$V = V_{str} + V_{harm} + V_{umb} \tag{1}$$

The mathematical expressions for the terms was given in the original paper and they will not be repeated here. It is, however, important to note that V_{str} is the stretching term given by

$$V_{str} = \sum_{i=1}^{3} V_3(R_{NH_i}, R_{NO}, R_{OH_1}) \tag{2}$$

where H_1 is the abstracted hydrogen and V_3 represents the London−Eyring−Polanyi (LEP) functional form used by Joseph et al.[22] This term explains the denomination "LEP-type" surface used for the polyatomic systems in this work. The term V_3 involves a singlet curve depending on three parameters ($^1D_{X-Y}$, α_{X-Y}, and R^e_{X-Y}) and a triplet curve depending on five parameters ($^3D_{X-Y}$, β_{X-Y}, c_{X-Y}, a_{X-Y}, and R^e_{X-Y}) for each bond X−Y. The N−H Morse parameter α_{N-H} is allowed to relax, using a switching function, from ammonia to amidogen radical

$$\alpha_{NH} = a_{NH} + b_{NH}\left(\frac{\tanh[c_{NH}(R - R^o)] + 1}{2}\right) \tag{3}$$

V_{harm} is a harmonic term for valence bends, written in a similar way to that in eq 6 of Jordan and Gilbert[23]

$$V_{harm} = \frac{1}{2}\sum_{i=1}^{2}\cdot\sum_{j=i+1}^{3} K^o K_i K_j (\theta_{ij} - \theta^o_{ij})^2 \tag{4}$$

The force constants K are adjustable parameters, and the reference angle θ^o_{ij} represents the equilibrium angle defined by the N−H bonds in ammonia, and is also allowed to relax using a switching function from ammonia to amidogen radical.

V_{umb} is the "umbrella bend potential" term, added to the surface to correct the umbrella mode of ammonia

$$V_{umb} = \sum_{i=1}^{3} f_{\Delta i} \sum_{j=1, j\neq i}^{3} {\Delta_{ij}}^2 + \sum_{i=1}^{3} h_{\Delta i} \sum_{j=1, j\neq i}^{3} {\Delta_{ij}}^4 \tag{5}$$

where

$$\Delta_{ij} = \cos^{-1}\left[\frac{(q_j - q_i)x(q_k - q_i)}{||(q_j - q_i)x(q_k - q_i)||}\cdot\frac{r_i}{||r_i||}\right] - \phi^o_{ij} \tag{6}$$

with $(q_j - q_i)$ and $(q_k - q_i)$ being two vectors between the three ammonia hydrogens and r_i the vector between the nitrogen and each of the hydrogens; f and h are adjustable parameters to obtain a correct description of the umbrella mode at ammonia.

It is necessary to note that the V_{str}, V_{harm}, and V_{umb} terms are wholly symmetric with respect to the permutation of the three hydrogens of ammonia. As pointed out by Jordan and Gilbert,[23] an asymmetric hydrogen treatment is an inconvenient feature if the analytical surface is to be used for trajectory calculations.

Finally, one must note that the LEP-type surface presents a $N-H_1-O$ collinear approach (180°), which is a typical behavior of the LEP-type surfaces, and one of their major disadvantages.

2.1. Calibration of the Analytical PESs. Having selected the functional form, we then calibrated the two electronic states of $^3A'$ and $^3A''$ symmetries as independent PESs. We used two calibration criteria, each with its particular objective. In the first case, the "linear" LEP-type PESs were calibrated to reproduce the geometries, frequencies and barrier heights of the "bent" ab initio calculations to make a more direct comparison between the surfaces, on both the $^3A'$ and $^3A''$ symmetries. These LEP-type surfaces will be denoted S1 ($^3A'$ and $^3A''$). The calibration process used in this work thus consists of two steps. In the first step, we change the parameters (R^e_{X-Y}, $^1D_{X-Y}$, α_{N-H}, and α_{O-H}) of the PES to reproduce the geometric, energetic, and vibrational properties of the reactants and hydrogen-bonded complex (HBP). In a second step, we refit some parameters ($^3D_{X-Y}$, α_{N-O}) in order to reproduce the characteristics of the ab initio calculated saddle points (geometry, vibrational frequencies, and barrier height) for the $^3A'$ and $^3A''$ symmetries.

In the second case, theoretical and experimental information is taken into account in the calibration process. Besides the theoretical data on geometries, frequencies and barrier heights previously used in the S1 surface calibration, we use the reproduction of the experimental H-transfer rate constants as calibration criterion. Note that the final rate constant is obtained from the sum of the rate constants on the $^3A'$ and $^3A''$ surfaces, and thus it is necessary to refit some of the previous parameters. These LEP-type surfaces will be denoted S2 ($^3A'$ and $^3A''$).

The results of the final fits are listed in Table 1 for reactants, hydrogen-bonded complexes, and saddle points ($^3A'$ and $^3A''$). In general, the reactant properties (the only properties directly comparable with experiment) show reasonable agreement with experimental[24] data. The HBP geometry also shows reasonable agreement with the ab initio calculations, although the PES has a shorter $N-H_1$ bond. The vibrational frequencies are lower than the ab initio values, but it is well-known that ab initio calculations overestimate frequencies. This fact explains the difference in zero-point energy (ZPE) values. Finally, the

TABLE 1: Reactant, Hydrogen-Bonded Complex (HBP), and Saddle Point Properties[a]

	NH_3		HBP		$^3A'$			$^3A''$		
	PES	exptl[b]	PES	ab initio[c]	S1[d]	S2[d]	ab initio[c]	S1[d]	S2[d]	ab initio[c]
					Geometry					
$R(NH_1)$	1.011	1.012	1.885	2.024	1.275	1.275	1.200	1.293	1.298	1.220
$R(OH_1)$			0.980	0.978	1.106	1.103	1.175	1.098	1.087	1.116
$\angle NH_1O$			180.	180.	180.	180.	159.5	180.	180.	144.4
$R(NH_i)$	1.011	1.012	1.013	1.021	1.013	1.013	1.020	1.013	1.013	1.020
$\angle H_1NH_i$	106.7	106.7	80.2	127.7	105.7	105.7	103.3	105.4	105.3	106.1
					Frequency					
	3541[e]	3577[e]	3600	3716	3462	3463	3631	3454	3432	3644
	3433	3506	3287	3630	3417	3418	3517	3412	3393	3535
	1701[e]	1691[e]	3270	3512	1627	1627	1630	1618	1614	1662
	1000	1022	1443	1595	1360	1356	1600	1319	1295	1513
			571	601	956	954	1300	943	939	1222
			330	554	676	685	847	703	755	882
			287	211	503	500	586	495	476	528
			255	192	487	482	513	481	458	506
			162	165	1884i	1835i	1724i	1710i	1476i	1304i
					Energy					
ΔE	0.0		3.6	2.7[g]	15.1	14.6	15.1[g]	13.9	12.0	13.9[g]
ΔH (0 K)	0.0		0.9	0.7	11.5	11.0	12.3	10.1	8.01	10.9
ZPE[f]	21.5	21.5	18.8	20.3	17.8	17.8	19.5	17.8	17.7	19.3

[a] Distances in angstrom, frequencies in cm^{-1}, energies in kcal mol^{-1}. [b] Reference 24. $NH_3(C_{3v})$. [c] Second-order Møller−Plesset perturbation theory calculations, from ref 2. [d] S1 is the PES from this work to reproduce the ab initio barrier height, and S2 is the PES from this work to reproduce the experimental H abstraction rate constants. [e] Doubly degenerate. [f] Harmonic zero-point energy in kcal mol^{-1}. The harmonic ZPE is one-half the sum of the frequencies for the bound modes. [g] Energies obtained as single-point CCSD(T)/AUG-cc-pVTZ//MP2/6-31G(d,p) (level 2) from ref 2.

difference of enthalpy at 0 K (0.9 kcal mol^{-1}) agrees with the ab initio value.

Next, we consider the saddle point properties. When the $O(^3P)$ approaches the NH_3 with C_s symmetry, two electronic states of symmetries $^3A'$ and $^3A''$ are obtained. In our previous work[2] we found that the $^3A''$ saddle point is 1.2 kcal mol^{-1} more stable than the $^3A'$ saddle point, and both stationary points are "bent", with $N-H_1-O$ angles of 144.4° ($^3A''$) and 159.5° ($^3A'$). Comparison of the properties of the saddle point of these LEP-type surfaces with ab initio calculations shows that these surfaces reproduce the trends and values, although the new surfaces present a collinear approach (180°). Each saddle point ($^3A'$ and $^3A''$) has one imaginary frequency, whose value is larger than the corresponding ab initio result. The S1 PESs ($^3A'$ and $^3A''$), used in this work to reproduce the barrier height of the "bent" ab initio calculations, maintain the same energy difference (1.2 kcal mol^{-1}) as in the ab initio results, and for each surface the combined effect of potential energy and ZPE, i.e., $\Delta H_o^{\neq}$, the conventional transition-state enthalpy of activation at 0 K, is close to, although smaller than, the ab initio calculation. The S2 PESs ($^3A'$ and $^3A''$), used in this work to reproduce the experimental H-transfer rate constants, present a similar behavior, although it was necessary to modify the individual barrier heights.

2.2. Dynamical Calculations. With the new "linear" LEP-type $^3A'$ and $^3A''$ surfaces calibrated as described in the previous section, the reaction paths were independently calculated starting from the respective saddle point geometry and going downhill to both reactants and HBP in mass-weighted Cartesian coordinates, using Page and McIver's method[25] with a step-size of 0.001 $amu^{1/2}$ bohr. The Hessian matrix was evaluated every 10 points along this reaction path. Along this minimum energy path (MEP), the reaction coordinate s is defined as the signed distance from the saddle point, with $s > 0$ referring to the product side. In the rest of this paper, the units of s are bohr, and all calculations are carried out in mass-scaled coordinates with a reduced mass μ equal to 1 amu. Thus, distances in mass-scaled coordinates in bohr are equivalent to distances in mass-weighted coordinates in $amu^{1/2}$ bohr. We calculated the reaction path between $s = -2.5$ bohr and $s = +2.5$ bohr. All the rate constants converged well with respect to the gradient step-size, the distance between Hessian the matrices (0.01 bohr), and the extent of the reaction path calculated.

Along each MEP a generalized normal-mode analysis was performed using a curvilinear projection operator[26] formalism. With this information, we calculated, first, the ground-state vibrationally adiabatic potential curve

$$V_a^G(s) = V_{MEP}(s) + \epsilon_{int}^G(s) \quad (7)$$

where $V_{MEP}(s)$ is the classical energy along the MEP with its zero energy at the reactants ($s = -\infty$), and $\epsilon_{int}^G(s)$ is the zero-point energy at s from the generalized normal-mode vibrations orthogonal to the reaction coordinate, and second, the coupling terms[27] $B_{k,F}(s)$ measuring the coupling between the normal mode k and the motion along the reaction coordinate, mode F. These coupling terms are the components of the reaction-path curvature $\kappa(s)$, defined as

$$\kappa(s) = \left(\sum [B_{k,F}(s)]^2\right)^{1/2} \quad (8)$$

and they control the nonadiabatic flow of energy between these modes and the reaction coordinate.[28,29] These coupling terms will allow us to calculate accurate semiclassical tunneling factors, and to give a qualitative explanation of the possible vibrational excitation of reactants and/or products, i.e., dynamical features, which are another sensitive test of the new surfaces.

Finally, the energies, vibrational frequencies, geometries, and gradients along each MEP were used to estimate rate constants by using variational transition state theory (VTST). We calculated thermal rates using the canonical variational theory[30,31] (CVT) approach which locates the dividing surface between reactants and products at a point $s_*^{CVT}(T)$ along the reaction path that minimizes the generalized TST rate constants $k^{GT}(T,s)$ for a given temperature T. Thermodynamically, this is equivalent to locating the transition state at the maximum $\Delta G^{GT,o}$

$[T,s_*^{CVT}(T)]$, of the free energy of activation profile $\Delta G(T,s)$.[30,31] Thus, the thermal rate constant will be given by

$$k^{CVT}(T) = \sigma\frac{k_B T}{h}K^o \exp[-\Delta G(T,s^{*,CVT})/k_B T] \qquad (9)$$

with k_B being Boltzmann's constant, h being Planck's constant, σ being the symmetry factor (the number of equivalent reaction paths, which were assumed to be 3 and 2 for the forward and reverse reactions, respectively), and K^o being the reciprocal of the standard-state concentration, taken as 1 molecule cm^{-3}.

The analysis of the $V_a^G(s)$ curves showed the existence of two maxima for each of the $^3A'$ and $^3A''$ surfaces, and the rate constants were therefore finally calculated using the canonical unified statistical model (CUS).[31,32]

In the present work, we used the general polyatomic rate constants code POLYRATE.[33] The rotational partition functions were calculated classically, and the vibrational modes were treated as quantum mechanical separable harmonic oscillators, with the generalized normal-modes defined in redundant curvilinear coordinates.[26] The chosen curvilinear coordinates were all the possible bond lengths and bond angles. The advantage of curvilinear coordinates (nonlinear functions of Cartesian coordinates) over rectilinear ones (linear functions of Cartesian coordinates) is that in some cases the lowest bending frequencies had unphysical imaginary values over a wide range of the reaction coordinate using rectilinear coordinates, whereas these frequencies were real over the whole of the reaction path using curvilinear coordinates. This behavior has been verified in this reaction and other hydrogen abstraction reactions.[34−37] In calculating electronic partition functions, we included the spin−orbit splitting of $O(^3P)$, which is 158.26 and 226.98 cm^{-1} for $^3P_1$ and ^3P_o relative to $^3P_2$.

Finally, we considered the tunneling contributions. This reaction has a heavy−light−heavy mass combination, and therefore, a large curvature tunneling (LCT) calculation should be considered.[38] In this case we used the new version LCG-4, recently developed by Fernández-Ramos and Truhlar,[39] which treats the anharmonic potentials encountered along low-energy corner-cutting tunneling paths more accurately than the previous LCG-3 version.[38] We used the microcanonical optimized multidimensional tunneling (μOMT) approach[40] in which, at each total energy, the larger of the SCT (small curvature tunneling) and LCT tunneling probabilities is taken as the best estimate. In the LCT calculations we allowed the system to reach all the accessible vibrational excited states into which tunneling proceeds.[38,39] Finally, the total rate constant is obtained from the sum of the calculated rate constants on the $^3A'$ and $^3A''$ surfaces.

3. Results and Discussion

We begin by comparing the results of the kinetics and dynamics for the ab initio calculations (bent surfaces) and the S1 surfaces (linear surfaces), which display (from the calibration criterion) similar barrier heights.

3.1. Reaction-Path and Frequency Analysis. As in the "bent" ab initio calculations,[2] the two "linear" LEP-type S1 surfaces ($^3A'$ and $^3A''$) have a similar shape, so that henceforth we will refer only to the more stable $^3A''$ surface. Classical energies along the MEP, V_{MEP}, and ground-state vibrationally adiabatic potential energy curves, ΔV_a^G, as a function of s are plotted in Figure 1 for the ab initio and S1 surfaces. Note that ΔV_a^G is defined as the difference between this magnitude at s and its value for the reactants. The barrier height is reproduced

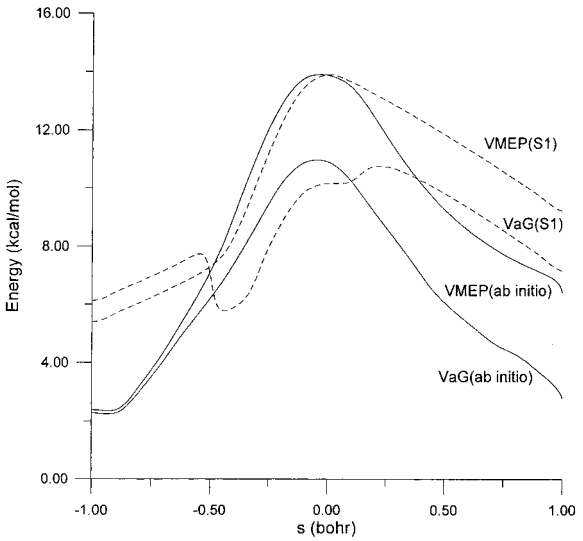

Figure 1. Classical potential energy curves V_{MEP} and vibrationally adiabatic potential energy curves ΔV_a^G as a function of s for the "bent" ab initio (solid line) and "linear" S1 (dashed line) surfaces.

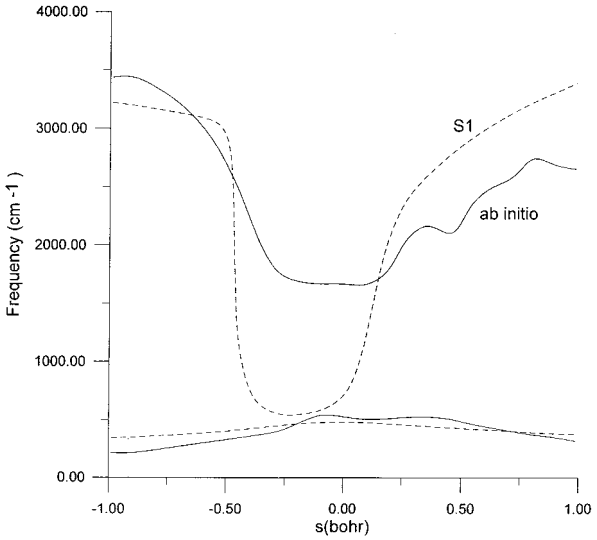

Figure 2. Some generalized normal-mode vibrational frequencies plotted vs the reaction coordinate for the ab initio (solid line) and S1 (dashed line) surfaces. The lowest frequencies for both surfaces are very similar and only one is shown in each case.

(calibration criterion), but there is a sharper fall off to both the asymptotic reactants and products channels in the case of the ab initio MEP. In this last case, the energy effects dominate on the entropy effects, and the shape of the ab initio V_a^G curve is similar to the shape of the V_{MEP} curve. In the LEP-type S1 surface, the greater flatness of the MEP means that the entropy effects are more pronounced, and this leads to a very different V_a^G curve, with two peaks.

The vibrational frequencies with the sharpest changes along the MEP are shown in Figure 2 for the ab initio (solid line) and S1 (dashed line) surfaces. The most important change corresponds to the mode related to the breaking $(N-H_1)$/forming (H_1-O) bonds (*reactive mode*). This mode presents a widening of the vibrational well, an effect which has been found in other reactions with a small skew angle.[41−43] The two lowest bending modes along the reaction path (*transitional modes*) correspond to the transformation of free rotations or free translations of the reactant limit into real vibrational motions in the overall system. Their frequencies tend asymptotically to zero at the reactant and product limits and reach their maxima in the saddle

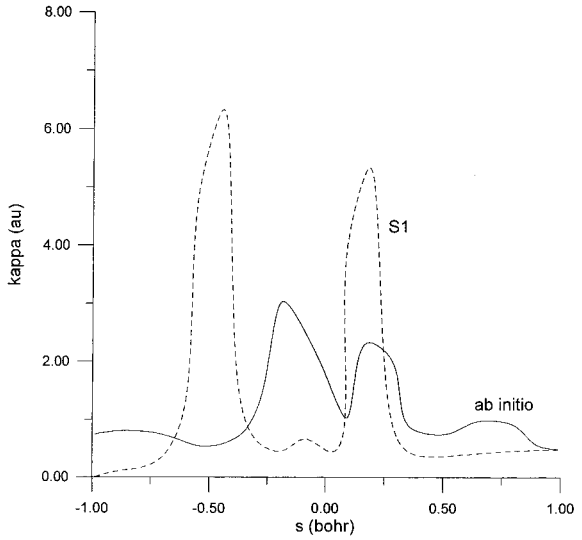

Figure 3. Reaction-path curvature (κ) as a function of s for the "bent" ab initio (solid line) and "linear" S1 (dashed line) surfaces.

point zone. It is interesting to note that the ab initio and the S1 surfaces show similar behavior for both symmetric stretching and bending modes, although there is a sharper fall off for the S1 surface.

Further analyzing the reaction valley, the curvature term (κ) along the reaction path as a function of s is plotted in Figure 3 for the ab initio (solid line) and S1 (dashed line) surfaces. The two surfaces show two sharp peaks, one on the reactant side due to strong coupling of the reaction path to the NH_3 reactive stretch and umbrella modes. Excitation of these modes might be expected to enhance the forward reaction rates. The second peak is in the exit channel and is lower than the first. It is essentially due to the coupling of the reaction path to the OH stretching mode with very small contributions from the NH_2 bending modes. This might be an indication that the OH stretching and the NH_2 bending modes could appear vibrationally excited for thermal reactions. However, as was already mentioned in our previous paper,[2] because of the stability of the hydrogen-bonded complex (HBP) formed, a randomization of the energy will lead to OH and NH_2 excitations smaller than those in other direct reactions without the possibility of such an effective randomization. Unfortunately, comparison with experiment is not possible. This analysis provides 2-fold information. It shows first that the reaction-path curvature must be taken into account in order to calculate the tunneling effect, and second illustrates the nonadiabatic flow of energy between these modes and the reaction coordinate. In summary, the two surfaces ("bent" ab initio and "linear" S1) display similar dynamic behavior, although the S1 peaks are displaced to the reactant channel and are larger.

3.2. Rate Constants. In the canonical version of VTST, CVT, the dividing surface is varied along the reaction path to minimize the rate constants, giving the generalized transition-state (GTS) at the value s*. Continuing with the ab initio ("bent" surface) and S1 ("linear" surface) comparison, the analysis of the ΔV_a^G curves (Figure 1) showed the existence of one maximum for the ab initio surface, but two maxima for the S1 surface. In this latter case, the rate constants were therefore finally calculated using the canonical unified statistical model (CUS).[31,32] The bottleneck properties of the reaction for the S1 surface, based on the CVT approach, show that the location of the GTS is from +0.215 to +0.208 bohr for the $^3A''$ electronic state over the temperature range 500−2000 K, respectively. Note that this location with the ab initio surface[2] was very close to the saddle point: from −0.060 to −0.012 bohr, for the same temperature range. Therefore, the variational effects, that is, the ratios between variational CVT and conventional TST rate constants, are larger for the S1 surface.

TABLE 2: Forward Rate Constants[a] for the $NH_3 + O(^3P)$ Reaction with a Barrier Height of 13.9 kcal mol^{-1}

	$^3A''$ surface				total: $^3A' + {}^3A''$		
	ab initio[b]		S1[c]		ab initio[b]	CUS/SCT	
T(K)	CVT	SCT	CUS	SCT	CVT/SCT	SI[c]	exptl[d]
500	1.71(−16)[e]	23.82	2.43(−16)	2.09	4.32(−15)	6.35(−16)	3.84(−15)
600	1.19(−15)	10.72	1.60(−15)	1.67	1.39(−14)	3.57(−15)	1.74(−14)
700	4.97(−15)	6.33	6.33(−15)	1.46	3.57(−14)	1.31(−14)	5.10(−14)
1000	7.70(−14)	2.74	8.55(−14)	1.21	2.66(−13)	1.65(−13)	3.82(−13)
1500	8.59(−13)	1.63	7.84(−13)	1.09	2.00(−12)	1.26(−12)	2.50(−12)
2000	3.42(−12)	1.33	2.67(−12)	1.05	6.94(−12)	4.55(−12)	6.39(−12)

[a] In cm^3 molecule^{-1} s^{-1}. [b] Ab initio rate constants from ref 2. [c] This work, on the S1 surface. [d] Experimental values are from ref 14 (at intermediate temperatures, 500−800 K) and from ref 18 (at high temperatures, 1000−2000 K). [e] 1.71(−16) stands for 1.71×10^{-16}.

We also compared the tunneling contribution for the ab initio and S1 surfaces. Since for the ab initio case[2] we only had information on the reaction path, for this comparison we used the centrifugal-dominant small-curvature tunneling method (SCT),[44] common to both surfaces. Table 2 lists the variational rate constants and SCT tunneling contribution for the ab initio and S1 surfaces, respectively, over the temperature range 500−2000 K, where the rate constant for the $^3A''$ electronic state and the total rate constant (for the $^3A'$ and $^3A''$ curves) are listed separately. We shall begin by analyzing the rate constants for the $^3A''$ electronic state, which permits us to separate the variational contribution from the tunneling effect. The CVT and CUS values are similar over all the temperature range, with differences being by a factor of about 1.3−1.4. However, the SCT tunneling contribution is very different, with differences from 11.4 to 1.3 over the temperature range 500−2000 K, respectively. The explanation of this large difference is the narrower shape of the ab initio MEP with respect to the S1 MEP (Figure 1). From our previous experience with H-transfer reactions where the heavy−light−heavy mass combination is present, we conclude that the SCT values for the ab initio surface are overestimated. Thus, for example at 500 K, the SCT values are: $NH_3 + OH$, 1.38;[45] $CH_4 + Cl$, 1.15;[46] and $CH_4 + O(^3P)$, 1.50.[37] The value 2.09 obtained with the S1 surface is consistent with these results, and lends confidence to the MEP shape of the S1 surface in Figure 1.

With respect to the total rate constants ($^3A'$ and $^3A''$), the agreement between the ab initio surfaces and the experimental values can be explained as being due to the overestimated tunneling effect. The S1 surfaces yield smaller rate constants over all the temperature range. However, it is encouraging that both ab initio and S1 surfaces show a similar behavior of the rate constants vs temperature, although the only calibration criterion used for the S1 surfaces was to reproduce the ab initio barrier heights.

For comparison purposes, and in light of the poor agreement obtained with the S1 surfaces, especially at low temperatures (as could be expected from the very restricted calibration criterion imposed), we refitted some parameters for the $^3A'$ and $^3A''$ surfaces, independently, to reproduce the experimental rate constants and the ab initio saddle point properties. Obviously, the goal now is not to study kinetic parameters (which are obtained by the calibration criterion), but to propose an analytical surface which is of utility for dynamic studies. We thereby

TABLE 3: Rate Constants without Tunneling (k) and Transmission Coefficients (κ) for the $NH_3 + O(^3P)$ Reaction on the S2-$^3A''$ Surface

	k		κ			
T(K)	CVT	CUS	SCT	LCG3[a]	LCG4[b]	μOMT
500	1.76(−15)[c]	1.63(−15)	1.87	5.35	2.09	2.27
600	8.74(−15)	7.71(−15)	1.55	3.11	1.62	1.73
700	2.87(−14)	2.42(−14)	1.38	2.25	1.40	1.49
1000	2.86(−13)	2.17(−13)	1.17	1.45	1.17	1.21
1500	2.25(−12)	1.46(−12)	1.07	1.17	1.07	1.08
2000	7.47(−12)	4.31(−12)	1.04	1.05	1.04	1.04

[a] Large curvature tunneling method, version 3. Reference 38. [b] Large curvature tunneling method, version 4. Reference 39. [c] 1.76(−15) stands for 1.76×10^{-15}. In cm^3 molecule^{-1} s^{-1}.

TABLE 4: Total Forward Rate Constants[a] for the $NH_3 + O(^3P)$ Reaction

	S2	ab initio	
T(K)	CUS/μOMT	CVT/SCT	exptl[b]
500	4.03(−15)[c]	4.32(−15)	3.84(−15)
600	1.51(−14)	1.39(−14)	1.74(−14)
700	4.24(−14)	3.57(−14)	5.10(−14)
1000	3.46(−13)	2.66(−12)	3.82(−12)
1500	2.12(−12)	2.00(−12)	2.50(−12)
2000	6.59(−12)	6.94(−12)	6.39(−12)

[a] In cm^3 molecule^{-1} s^{-1}. [b] Experimental values are from ref 14 (at intermediate temperatures, 500−800 K) and from ref 18 (at high temperatures, 1000−2000 K). [c] 4.03(−15) stands for 4.03×10^{-15}.

obtained the "linear" LEP-type S2 surfaces ($^3A'$ and $^3A''$). To analyze the tunneling contribution, we shall begin by studying the rate constants for the $^3A''$ electronic state (Table 3). Comparison of columns 2 and 3 shows recrossing effects in the thermal rate constants, increasing from a factor of 1.08 at 500 K to a factor of 1.73 at 2000 K. The small SCT transmission coefficients agree with the values for the S1 surface (Table 2) and with other heavy−light−heavy reactions.[37,45,46] A comparison between versions 3, LCG-3,[38] and 4, LCG-4,[39] of the large curvature tunneling effect shows that LCG-3 is overestimated with respect to the new version, by factors of from 2.56 at 500 K to 1.00 at 2000 K. This result agrees with the conclusion of Fernández-Ramos and Truhlar[39] that there appears to be a significant error in the way that the LCG-3 algorithm calculates low-energy tunneling probabilities.

Table 4 lists the variational CUS/μOMT total rate constants ($^3A'$ and $^3A''$). together with the experimental and other theoretical rate constants, for the temperature range 500−2000 K for the forward reaction (Figure 4). The S2 surfaces also present curvature in the Arrhenius plot (the expected behavior in a reaction with a heavy−light−heavy mass combination), although less marked than in the previous ab initio calculations.

A priori, the agreement between the LEP-type S2 aurface and the ab initio rate constants might seem surprising, given that the two surfaces are so different. In our previous paper on the ab initio surfaces[2] we first constructed the reaction paths at a moderate level of calculation (second-order Møller−Plesset perturbation theory) which overestimates the barrier heights by 6.3 and 5.3 kcal mol^{-1} for the $^3A'$ and $^3A''$ surfaces, respectively, with respect to a higher level of calculation (which includes more correlation energy and uses a larger basis set). Thus, in a second step, we had to optimize our ab initio reaction paths, scaling them by a constant factor to reproduce the barrier heights of the higher level calculation. Note that this is a standard approach in the construction of reaction paths using electronic structure calculations. With this process, a reasonable agreement was obtained with the experimental rate constants. In the case

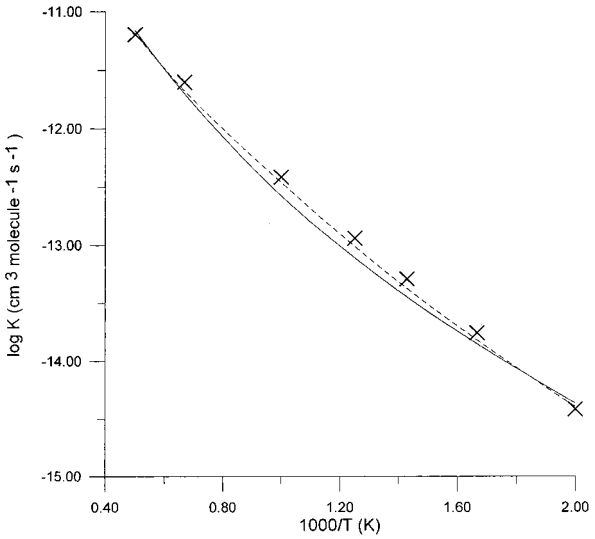

Figure 4. Arrhenius plot of log k (cm^3 molecule^{-1} s^{-1}) against the reciprocal of the temperature (K) in the range 500−2000 K. Experimental values (crosses) are from ref 14 (at intermediate temperatures, 500−800 K) and from ref 18 (at high temperatures, 1000−2000 K). Ab initio results (solid line) from ref 2. Dashed line, this work on the S2 surfaces ($^3A'$ and $^3A''$).

TABLE 5: Theoretical and Experimental Activation Energies (kcal mol^{-1})

ΔT(K)	ab initio[a]	S2[b]	exptl
361−677	6.44	7.35	6.60[c]
448−841	6.32	8.27	9.00[d]
765−1790	11.37	10.81	11.15[e]
1750−2060	15.64	13.97	8.88[f]

[a] Reference 2. [b] This work. [c] Kurylo et al. (361−677 K). Reference 11. [d] Perry (448−841 K). Reference 14. [e] Sutherland et al. (765−1790 K). Reference 18. [f] Salimian et al. (1750−2060 K). Reference 4.

of the analytical potential energy surface S2, note that this surface is explicitly calibrated to reproduce the experimental data.

Table 5 lists the phenomenological activation energies computed as local slopes of the Arrhenius plot for the forward reaction. The activation energy can be obtained from the total rate constants through the usual definition

$$E_a = -R\, \mathrm{d}(\ln k)/\mathrm{d}(1/T) \qquad (10)$$

which is equivalent to determining the slope of the plot in Figure 4. At low (448−841 K) and intermediate temperatures (765−1790 K), the theoretical results are close to the more recent experimental values of Perry[14] and Sutherland et al.,[18] respectively; but they markedly disagree with the experimental result of Salimian et al.[4] at high temperatures (1750−2060 K). However, as was remarked in the Introduction, the rate constants given by this group presented uncertainties of a factor of 4, so that with these theoretical results it appears that the experimental value is questionable.

Finally, to make a quantitative estimate of the role of the tunneling in the curvature of the Arrhenius plot, we fitted the S2 results to a three-term expression of the type $AT^m \exp(-B/T)$. The resulting equation is

$$k(T) = 1.14 \times 10^{-18}\, T^{2.24} \exp(-2880/T), \quad \mathrm{cm^3\ molecule^{-1}\ s^{-1}} \qquad (11)$$

which agrees with experimental evaluations,[5,20] and shows a

lower degree of curvature ($T^{2.24}$) in the Arrhenius plot than our previous ab initio fit[2] ($T^{2.93}$).

4. Conclusions

This work is the second of a series designed to examine whether the popular LEPS surface can be used to describe the kinetics and dynamics of systems with noncollinear reaction paths. In the first paper of the series, we analyzed the atom−diatom Cl + HCl system (ClHCl angle = 168.4°). In this second paper, using as a test bed the polyatomic $NH_3 + O(^3P)$ system, which presents a nonlinear conformation of the central atoms (NH_1O angle ≠ 180°), we compared the results for the kinetics and dynamics for an ab initio "bent" surface, previously constructed by our group using molecular orbital theory, with those for a simple "linear" LEP-type surface (S1) constructed and calibrated in this work. We found that the breaking/forming bonds, the maximum change in the stretching modes, the reaction-path curvature (an important factor related to the tunneling effect and the reaction coordinate-bound modes coupling), and the rate constants behave similarly for the two surfaces, taking into account the calibration criterion. This agreement is especially encouraging in this particular reaction because the approach of the $O(^3P)$ atom to ammonia with C_s symmetry proceeds via two electronic states of symmetries $^3A'$ and $^3A''$. This capacity of the LEP-type surface to reproduce the kinetics and dynamics of polyatomic systems with noncollinear reaction paths, generalizing the conclusions reached for triatomic systems by our group, is also encouraging, and represents a great saving in calculation time, since it is well-known that the complete construction of an analytical surface for polyatomic systems is no trivial task and is very time-consuming.

Acknowledgment. The author is very grateful to Dr. J. C. Corchado for many helpful discussions, and to Prof. D. G. Truhlar for providing a copy of the POLYRATE program. This work is supported in part by Consejeria de Educación, Ciencia y Tecnología, Junta de Extremadura, Spain (Project No. IPR99A009).

Standard Acronyms

CVT: Canonical variational theory

CUS: Canonical unified statistical (model)

$^1D_{X-Y}$, α_{X-Y}, R^e_{X-Y}: Morse parameters for the singlet two-body potentials used in eq 2. Adjustable parameters in the calibration process.

$^3D_{X-Y}$, β_{X-Y}, R^e_{X-Y}: Morse parameters for the triplet two-body potentials used in eq 2. Adjustable parameters in the calibration process.

GTS: Generalized transition-state.

HBP: Hydrogen-bonded complex located in the product channel.

HLH: Heavy−light−heavy mass combination. Its presence in the reactive system indicates possibility of tunneling.

LCT: Large curvature tunneling, which is obtained in this paper using two methods, LCG-3 and LCG-4, which differ in the way that low-energy tunneling probabilities are calculated.

LEPS: London−Eyring−Polanyi−Sato analytical potential energy surface, widely used for the kinetic and dynamic study of triatomic systems.

LEP: London−Eyring−Polanyi analytical potential energy surface, used as starting point for polyatomic systems with the suitable modifications. Hence, the denomination LEP-type used in this paper.

MEP: Minimum energy path. In this paper it is equivalent to reaction path and intrinsic reaction coordinate (IRC).

SCT: Small curvature tunneling, which only uses information on the reaction path.

S1: Analytical potential energy surface calibrated in this work to reproduce theoretical information from ab initio calculations.

S2: Analytical potential energy surface calibrated in this work to reproduce theoretical information from ab initio calculations and experimental rate constants.

TST: Transition state theory.

VTST: Variational transition state theory.

References and Notes

(1) Espinosa-García, J. *J. Phys. Chem. A* **2001**, *105*, 134.
(2) Espinosa-García, J. *J. Phys. Chem. A* **2000**, *104*, 7537.
(3) Baldridge, K. M.; Gordon, M. S.; Steckler, R.; Truhlar, D. G. *J. Phys. Chem.* **1989**, *93*, 5107.
(4) Salimian, S.; Hanson, R. K.; Kruger, C. H. *Int. J. Chem. Kinet.* **1984**, *16*, 725; Hanson, R. K.; Salimian, S. In *Combustion Chemistry*; Gardiner, W. C., Ed.; Springer-Verlag: New York, 1985; Chapter 6, p 361.
(5) Cohen, N. *Int. J. Chem. Kinet.* **1987**, *19*, 319.
(6) Fenimore, C. P.; Jones, G. W. *J. Phys. Chem*. **1961**, *65*, 298.
(7) Wong, E. L.; Potter, A. E. *J. Chem. Phys*. **1963**, *39*, 2211.
(8) Aganesyan, K. T.; Nalbandyan, A. B. *Dokl. Akad. Nauk. SSSR*, **1965**, *160*, 62.
(9) Wong, E. L.; Potter, A. E. *J. Chem. Phys*. **1965**, *43*, 3371.
(10) Albers, E. A.; Hoyermann, K.; Wagner, H. Gg.; Wolfrum, J. *12th. Symp. (Int.) Combust.* **1969**, 313.
(11) Kurylo, M. J.; Hollinden, G. A.; LeFevre, H. F.; Timmons, R. B. *J. Chem. Phys*. **1969**, *51*, 4497.
(12) Kirschner, K.; Mergete, N.; Schmidt, C. *Chem. Ing. Tech.* **1974**, *46*, 661.
(13) Lalo, C.; Vermiel, C. *J. Chim. Phys*. **1980**, *77*, 131.
(14) Perry, R. A. *Chem. Phys. Lett*. **1984**, *106*, 223.
(15) Baulch, D. L.; Campbell, I. M.; Hainsworth, R. *J. Chem. Soc., Faraday Trans*. **1984**, *80*, 2525.
(16) Fujii, N.; Sato, H.; Fujimoto, S.; Hiyama, H. *Bull. Chem. Soc. Jpn.* **1984**, *57*, 277.
(17) Fujii, N.; Chita, K.; Uchida, S.; Hiyama, H. *Chem. Phys. Lett*. **1986**, *127*, 141.
(18) Sutherland, J. W.; Patterson, P. M.; Klemm, R. B. *J. Phys. Chem.* **1990**, *94*, 2471.
(19) Baulch, D. L.; Cobos, C. J.; Cox, R. A.; Esser, C.; Frank, P.; Just, Th.; Kerr, J. A.; Pilling, M. J.; Troe, J.; Walker, R. W.; Warnatz, J. *J. Phys. Chem. Ref. Data* **1992**, *21*, 439.
(20) Dean, A. M.; Bozzelli, J. W. In *Gas-Phase Combustion Chemistry*; Gardiner, W. C., Ed.; Springer-Verlag: New York, 2000; Chapter 2, p 125.
(21) Corchado, J. C.; Espinosa-García, J. *J. Chem. Phys.* **1997**, *106*, 4013.
(22) Joseph, T.; Steckler, R.; Truhlar, D. G. *J. Chem. Phys.* **1987**, *87*, 7036.
(23) Jordan, M. J.; Gilbers, R. G. *J. Chem. Phys.* **1995**, *102*, 5669.
(24) Chase M. W.; Davies, C. A.; Downey, J. R.; Frurip, D. J.; McDonald R. A.; Syverud, A. N., Eds. *JANAF Thermochemical Tables*, 3rd ed.; National Standard Reference Data Series 14; National Bureau of Standards: Washington, DC, 1985.
(25) Page, M.; McIver, J. W. *J. Chem. Phys*. **1988**, *88*, 922.
(26) Jackels, C. F.; Gu, Z.; Truhlar, D. G. *J. Chem. Phys*. **1995**, *102*, 3188.
(27) Miller, W. H.; Handy, N. C.; Adams, J. E. *J. Chem. Phys.* **1980**, *72*, 99.
(28) Morokuma, K.; Kato, S. In *Potential Energy Surfaces and Dynamics Calculations*; Truhlar, D. G., Ed.; Plenum: New York, 1981; p 243.
(29) Kraka, E.; Dunning, T. H. In *Advances in Molecular Electronic Structure Theory*; JAI: New York, 1990; Vol. I, p 129.
(30) Garrett, B. C.; Truhlar, D. G. *J. Am. Chem. Soc*. **1979**, *101*, 4534.
(31) Truhlar, D. G.; Isaacson, A. D.; Garrett, B. C. In *The Theory of Chemical Reactions*; Baer, M., Ed.; Chemical Rubber Co.:, Boca Raton, FL, 1985; Vol. 4.
(32) Garret, B. C.; Truhlar, D. G. *J. Chem. Phys.* **1982**, *76*, 1853.
(33) Corchado, J. C.; Chuang, Y. Y.; Fast, P. L.; Villá, J.; Hu, W. P.; Liu, Y. P.; Lynch, G. C.; Nguyen, K.; Jackells, C. F.; Melissas, V.; Lynch, B. J.; Rossi, I.; Coitiño, E. L.; Fernández-Ramos, A.; Steckler, R.; Garrett, B. C.; Isaacson, A. D.; Truhlar, D. G. POLYRATE, Version 8.5; University of Minnesota: Minneapolis, 2000.
(34) Espinosa-García, J.; Corchado, J. C. *J. Phys. Chem.* **1996**, *100*, 16561.
(35) Corchado, J. C.; Espinosa-García, J. *J. Chem. Phys.* **1997**, *106*, 4013.

(36) Corchado, J. C.; Espinosa-García, J.; Neto, O. R.; Chuang, Y. Y.; Truhlar, D. G. *J. Phys. Chem.* **1998**, *102*, 4899.
(37) Espinosa-García, J.; García-Bernáldez, J. C. *Phys. Chem. Chem. Phys.* **2000**, *2*, 2345.
(38) Truong, T. N.; Lu, D. h.; Lynch, G. C.; Liu, Y. P.; Melissas, V. S.; Stewart, J. J.; Steckler, R.; Garrett, B. C.; Isaacson, A. D.; González-Lafont, A.; Rai, S. N.; Hancock, G. C.; Joseph, T.; Truhlar, D. G. *Comput. Phys. Commun.* **1993**, *75*, 43.
(39) Fernández-Ramos, A.; Truhlar, D. G. *J. Chem. Phys.* **2001**, *114*, 1491.
(40) Liu, Y. P.; Lu, D. h.; González-Lafont, A.; Truhlar, D. G.; Garrett, B. C. *J. Am. Chem. Soc.* **1993**, *115*, 7806.
(41) Bondi, D. K.; Connor, J. N. L.; Garrett, B. C.; Truhlar, D. G. *J. Chem. Phys.* **1983**, *78*, 5981.
(42) Espinosa-García, J.; Corchado, J. C. *J. Chem. Phys.* **1994**, *101*, 8700.
(43) Espinosa-García, J.; Coitiño, E. L.; González-Lafont, A.; Lluch, J. M. *J. Phys. Chem.* **1998**, *102*, 10715.
(44) Natanson, G. A.; Garrett, B. C.; Truong, T. N.; Joseph, T.; Truhlar, D. G. *J. Chem. Phys.* **1991**, *94*, 7875.
(45) Corchado, J. C.; Espinosa-García, J.; Hu, W. P.; Rossi, I.; Truhlar, D. G. *J. Phys. Chem.* **1995**, *99*, 687.
(46) Corchado, J. C.; Truhlar, D. G.; Espinosa-García, J. *J. Chem. Phys.* **2000**, *112*, 9375.